

Numerical and experimental investigations of personal ventilation system in a cubicle

Mohammad Youssef Al Hashem¹, Ahmad Habib²

^{1, 2} *Department of Power Engineering, Faculty of Mechanical Engineering, University of Aleppo*

Abstract: *In this work, a numerical model was constructed to simulate the flow in a cubicle. This model was able to predict the physical phenomena and calculate the thermal comfort quantities correctly. An additional library was added to the software and used to calculate the age of the air, the cooling efficiency and the predicted mean vote PMV. The numerical model was validated after performing a mesh independence study by comparing its basic flow parameters with a valid numerical results, the average relative error in the temperature profile was 0.56%. An experimental model was also proposed and validated by comparing its results with experimental results, the average relative error in the temperature profile was 1.01%.*

Keywords: *OpenFOAM, personal ventilation, age of air, thermal comfort.*

I. INTRODUCTION

1.1 Background

Thermal comfort and air quality are two important aspects of indoor environmental quality (IEQ). The heating, ventilating, and air-conditioning (HVAC) system determines energy and air exchange in buildings. Building occupants also participate in setting the room's environmental conditions by exchanging energy with the building. By the thermoregulatory process, the body core temperature is kept around 37°C [1], and the surface temperature varies between 29°C and 35°C [2, 3]. Since a temperature difference exists between the body surface and the ambient air, the buoyancy results in a thermal boundary around the human body moving upward. This thermal boundary layer around human body and the resulting thermal plume above it play a key role in the determination of the heat flux and the contaminant concentration distribution in the vicinity of the body.

In most buildings, clean and cool air is often supplied to an occupied space by both mixing and displacement ventilation systems. Often, occupants in rooms with mixing or displacement ventilation have to compromise between preferred thermal comfort and perceived air quality because some people are very sensitive to air movement while others are sensitive to the air quality. The disadvantage of the total volume ventilation principle is that often room air movement is changed due to furniture rearrangement, which may increase occupants' complaints of draught and/or poor air quality [4]. In contrast to total volume ventilation, personalized ventilation (PV) aims at supplying clean and cool outdoor air directly to the occupants. Kaczmarczyk [5] indicate that PV is capable of improving the thermal comfort and air quality around the subject, reducing the intensity of sick building syndrome (SBS) symptoms and thereby increasing subjects' productivity. Since personalized ventilation can satisfy the individual needs of each occupant by customizing the environment around the body, it has a big advantage over both displacement and mixing ventilations. It was also found that a PV system supplying an amount of fresh air four times smaller than the displacement ventilation could be more effective in terms of users' satisfaction [6, 7] and could also reduce cooling and heating power consumptions by approximately 75% and 61%, respectively [8]. The same conclusion was obtained by [4] that PV may decrease significantly the number of occupants

dissatisfied with inhaled air quality. The ability of PV to deliver clean, cool, and dry air to the breathing zone of each occupant and maintain the thermal comfort level depends on the interaction among the airflow generated by PV, occupant-initiated flows (free convection flow around the body and the flow of respiration), the airflow of exhalation, and the room airflow outside workspaces [9].

Several kinds of personalized ventilation devices have been developed recently. Some of them can improve the air quality as well as thermal comfort while others cannot. For example, a push-and-pull type of PV invented and applied to aircraft cabin seats showed a dramatic decrease (77%) of contaminant concentration inhaled by the exposure manikin when the local supply with clean air existed and the contaminant exhaled can only be exhausted effectively when the local exhaust and the local supply are used simultaneously [10]. A local exhaust ventilation system with a privacy cell in the air cabin developed by Dygert and Dang [11] also show an advantage compared to backseat exhaust, reducing the passenger exposure to 60% no matter where the infectious source is. Many personalized ventilation terminals have been developed and tested by Nielsen et al., and the performance of these systems proved significant [12-16].

1.2 Purpose

Recently the advantage of personalized ventilation system on fulfilling the indoor environment requirement and reducing energy consumption has been gradually accepted by people in practice. However, different layouts of PV were usually tested in the chambers, PV usually mounted in the cubicles with partition between them. This typical arrangement of the office spaces not only gives relatively independent environment on the remaining office space and other cubicles but allows the interaction between them. Depending on the configuration of the cubicle, layout of the furniture [17] and air distribution system, the environment in the cubicle, as well as around the manikin, may differ a lot and influence the thermal sensation and inhaled air quality in the breathing zone.

On the other hand, the commercial CFD codes – beside its high costs – aren't easily available in some countries. Also the open-source CFD codes are getting widely used in all research fields.

In this paper, an experimental and numerical investigation using the open-source CFD software OpenFOAM has been done. The results were compared with the experimental and numerical data founded in Kong et al. [18] in order to validate our experimental and numerical models. In addition, the predicted mean vote (PMV) and the mean age of air (AoA) were calculated to give a better understanding of the PV's thermal performance.

II. Method and procedure

2.1. Overview

The prototype room studied in [18] is an office room (625 cm × 1052 cm × 315 cm) with 12 cubicles arranged in 2 rows, located in the Syracuse Center of Excellent (CoE) Building (Fig. 1). Each cubicle has approximately the same configuration and size (191 cm × 184 cm × 171 cm). The target cubicle also contains a manikin. A grid mesh was created using Pointwise, and grid sensitivity was examined. The air and air contaminant movement in the cubicle was simulated by using STAR-CCM. The CFD model was validated by experimental results as well as verified by sensitivity analysis for model parameters. Analysis of the flow characteristics in the cubicle was conducted to quantify the driving forces and their respective impacts on the performance of the personalized ventilation. Cooling/heating efficiency and air quality index (AQI) [19] were calculated to evaluate the environmental quality and ventilation performance.



Fig.1: Prototype room [18]

The prototype in our study is an office room (1150 cm × 450 cm × 300 cm) with one cubicle that has the same dimensions and features as in [18], located at Aleppo University – Faculty of Mechanical Engineering (Fig. 2).



Fig.2: Overview of the prototype used in our study

The open-source CFD software OpenFOAM was used to simulate the flow field inside the cubicle and to estimate the predicted mean vote PMV and the mean age of air AoA, and both the numerical and experimental results were compared with Kong's data.

2.2. Experiment setup

Experiments were conducted to give us some basic ideas of the flow field as well as to validate the CFD model. The cubicle has the same dimensions and features as in Kong's experiments, the main dimensions of the cubicle in Kong's experiments were (191cm × 184 cm × 171 cm) with a 84 cm wide opening, the cubicle contained a front desk (74 cm × 177 cm), a side desk (152 cm × 58 cm), a computer and a PV supply vent located at 133.4 cm above the floor and 34 cm away from the front partition. The PV supply vent had the diameter of 6.9 cm, 36.8 cm long with two 11.4 cm long grill openings (Fig. 3).



Fig.3: PV supply vent used in [18]

During Kong’s test, a manikin in normal clothing (around 0.6 clo) was set a comfort mode, which resulted to the manikin could maintain the skin temperature at the temperature as in comfortable condition by controlling the heat flux. Both the temperature and heat flux of the manikin were monitored and recorded during the experiment, and the flow field around the manikin was monitored in terms of both velocity and temperature at different locations.

Temperature monitoring locations (left front, left, right front and right) at the heights (0.1 m, 0.6 m, 0.8 m, 1.1 m, 1.4 m, and 1.6 m) using the spherical anemometer with an accuracy of 0.02 m/s and 0.2°C. The velocity in front of the PV (location FC) was also measured to validate the CFD model at the heights (0.8 m, 1.1 m, 1.2 m, 1.4 m, 1.6 m) (Fig.4).

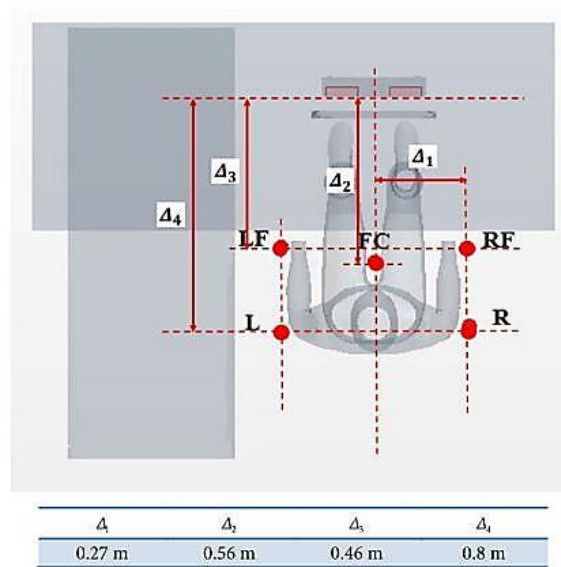


Fig.4: Monitoring locations [18]

As recently mentioned, the cubicle in this study has the exact same dimensions and features as in Kong’s research, the cubicle has a supply vent connected to circular duct with a diameter of 7.5 cm, the supply vent’s main dimensions are (7.4 cm × 16.4 cm) and it contains 6 horizontal blades and 10 vertical blades with actual area of 0.008496 m². The supply vent is located at 135 cm above the floor and 34 cm

away from the front partition (Fig. 5). The vent is supplied with cool air via a cooling device with the ability to control the air flow precisely (Fig. 6).



Fig.5: The supply vent

Instead of using a sophisticated thermal manikin, a real average shaped and average metabolic rate male with normal clothing (1.2 met, 0.6 col) was used in our experiments. The subject was in a comfortable situation during the experiments.

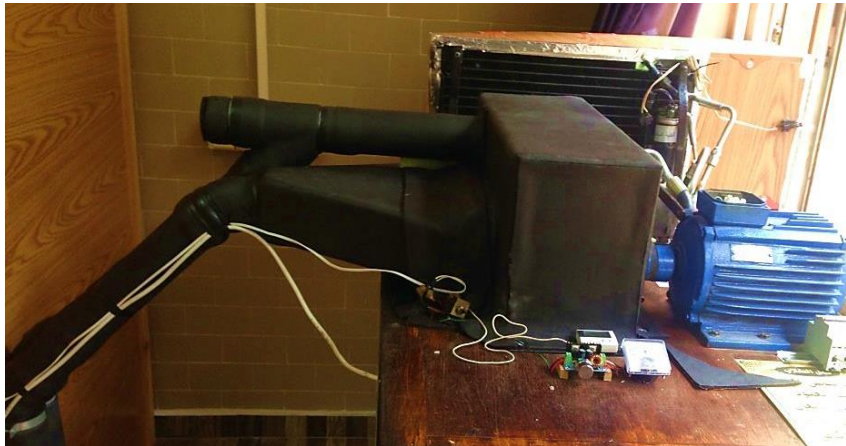


Fig.6: The cooling device

The flow field's temperature was monitored using a set of temperature controllers type Cheng KE CK-002, the sensors are NTC (Negative Temperature Coefficient) with accuracy of ± 0.5 °C and sensitivity of 0.1 °C. These temperature controllers were corrected and calibrated with a high accuracy mercury thermometer (Fig. 7).

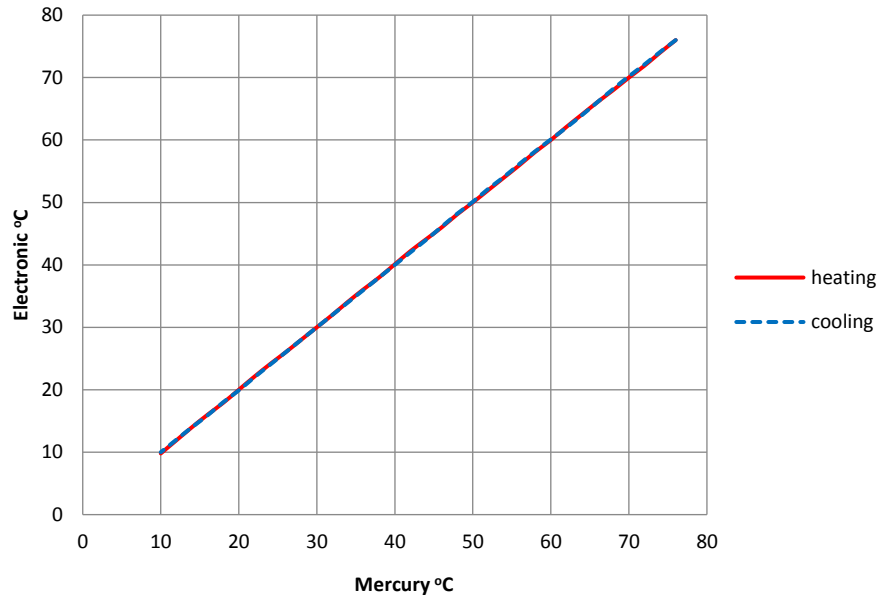


Fig.7: Temperature controller calibration diagram

To maintain the desired constant supply temperature, one temperature controller was utilized to control the compressor in the cooling device (Fig. 8).

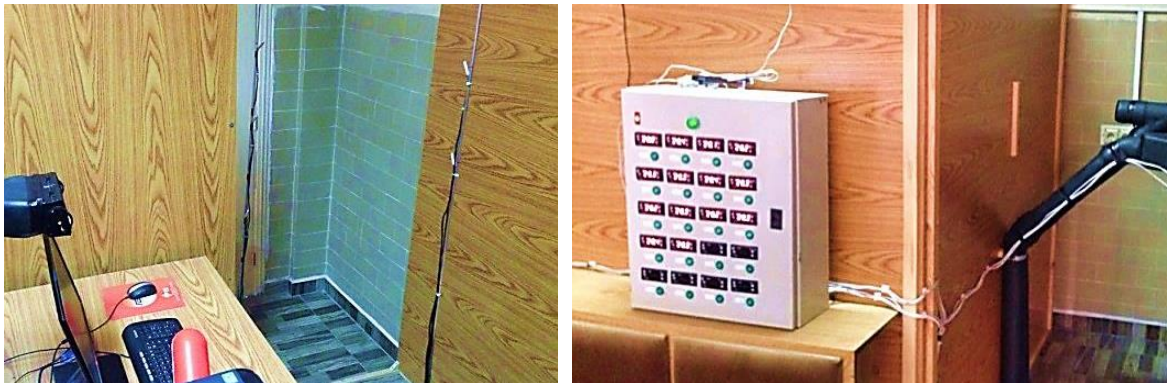


Fig.8: Temperature controllers and sensors

2.3. Governing equations for CFD model

The eddy-viscosity RANS model is the most popular class of turbulence model utilized for indoor environment simulations [3]. The basic equations include the transport equation of mass, momentum, and other quantities.

$$\frac{\partial}{\partial x_i}(\rho u_i) = 0 \tag{1}$$

$$\frac{\partial}{\partial t}(\rho u_j) + \frac{\partial}{\partial x_i}(\rho u_i u_j) = -\frac{\partial p}{\partial x_j} + \frac{\partial}{\partial x_i} \left(\mu \frac{\partial u_i}{\partial x_i} - \rho \overline{u'_j u'_i} \right) + S_j \tag{2}$$

$$\frac{\partial}{\partial t}(\rho\phi) + \frac{\partial}{\partial x_i}(\rho u_i \phi) = \frac{\partial}{\partial x_i} \left(\Gamma \frac{\partial \phi}{\partial x_i} - \rho \overline{u'_i \phi'} \right) + S \quad (3)$$

Boussinesq and Reynolds' analogies are used to model the turbulent term.

$$\tau_{ij} = -\rho \overline{u'_j u'_i} = \mu_t \frac{\partial u_i}{\partial x_j} \quad (4)$$

$$H_i = \rho C_p \overline{u'_i T'} = -\rho C_p \nu_t \frac{\partial T}{\partial x_i} \quad (5)$$

For RANS-based CFD methods, the most difficult task in setting up a CFD simulation is the selection of the turbulence model. Researchers have used a wide range of turbulence models when studying the microenvironment around the human body [3] including the zero- equation model [20], *standard k – ε* model [21, 22], the *RNG k– ε* model [23, 24], the *v2– f* model [25], the *realizable k– ε* model [26], and the *SST k– ω* model [27].

By comparing different turbulence models including *k– ε* family and *k– ω* family models, [3] found the *k– ε* family gave similar predictions and compared well with his test data, while *k– ω* turbulence models did not match with the test data in predicting the jet development. In this case the *realizable k– ε* turbulence model was used.

Another challenge in modeling room airflows by CFD is the simulation of flow close to solid surfaces since turbulent flow transits to laminar flow when it gets close enough to the surfaces. The two-layer approach, developed by [28], is used as an alternative to the low- Reynolds' number approach that allows the one-equation turbulence model to be applied in the near-wall region and the two-equation *k– ε* model to be applied in the region away from the wall. With this approach, the whole flow field is divided into two regions — the near-wall layer and the far field. In the near-wall layer, the turbulent kinetic energy *k* is calculated by

$$\frac{\partial k}{\partial t} + u_i \frac{\partial k}{\partial x_i} = d_k + P_k + G_k - \varepsilon \quad (6)$$

The eddy viscosity is calculated by

$$\nu_t = \sqrt{\overline{u'u'}} l_\mu \quad (7)$$

The turbulence dissipation rate ε by

$$\varepsilon = \frac{\sqrt{\overline{u'u'}} k}{l_\varepsilon} \quad (8)$$

Where G_k is the gravity production of turbulent kinetic energy, P_k is the shear production of the turbulent kinetic energy, and l_μ and l_ε are characteristic lengths that are defined in [29].

The values of ε specified in the near-wall layer are blended smoothly with the values computed from solving the *k– ε* equations far from the wall. The equation for turbulent kinetic energy is solved in the entire flow. This explicit specification of ε and μ_t is arguably no less empirical than the low-Reynolds' number approach, and the results are often as good or better than the *standard k – ε* results. In OpenFOAM, the two-layer formulations will work with either low-Reynolds' number type meshes $y^+ \sim 1$ or wall-function type meshes $y^+ > 30$ [30].

2.4. Post processing

In addition to the temperature and velocity fields, there are several quantities that can describe the thermal comfort situation. In order to calculate these quantities, a library had been added to the software code, this library (comfortFoam) was used to analyze the thermal comfort behavior based on EN ISO 7730 [31], and to calculate the predicted mean vote (PMV), predicted percentage of dissatisfaction (PPD) clothing temperature (T_{cl}), the mean radiant temperature T_{MR} and the age of air (AoA).

The predicted mean vote (PMV) was first proposed by Fanger [32], which can be represented on the ASHRAE 7-points thermal sensation scale, given in table 1. Fanger's PMV correlation is based on the identification of a skin temperature and sweating rate required for the optimal comfort conditions.

Table 1: ASHRAE 7-points thermal sensation scale

Value	Sensation
-3	Cold
-2	Cool
-1	Slightly cool
0	Neutral
1	Slightly warm
2	Warm
3	Hot

To quantify the index of air quality, IAQ, the concept of (Age of Air, AoA) which expresses the speed of air exchanges at a given point, is used. A low AoA value means that the air is often renewed, implying a good air quality. Additional differential transport equation (Eq. 9) of a scalar τ which represents the AoA [33] is solved.

$$\frac{\partial \tau}{\partial t} + \frac{\partial}{\partial x_i} (u_i \tau) - \frac{\partial}{\partial x_i} \left(\frac{\nu_{eff}}{\sigma_\tau} \cdot \frac{\partial \tau}{\partial x_i} \right) = 1 \quad (9)$$

Where

- The term $\frac{\partial \tau}{\partial t}$ represents the accumulation over time.
- The term $\frac{\partial}{\partial x_i} (u_i \tau)$ represents the transport of τ by advection.
- The term $\frac{\partial}{\partial x_i} \left(\frac{\nu_{eff}}{\sigma_\tau} \cdot \frac{\partial \tau}{\partial x_i} \right)$ represents the diffusion of τ .
- The right term is the source term which is equal to 1.

$\left(\frac{\nu_{eff}}{\sigma_\tau} \right)$ is the diffusion coefficient of the linear momentum, (ν_{eff}) adjusted by the dimensionless number (σ_τ) . Recall that the effective kinematic viscosity $\nu_{eff} = \nu_l + \nu_t$ is the sum of the molecular kinematic viscosity (ν_l), which is an intrinsic property of the fluid, and the turbulent kinematic viscosity (ν_t), which characterizes the turbulence of the flow in the first order of turbulence models. The dimensionless number (σ_τ) is the equivalent Prandtl number of τ and represents the ratio between the diffusion coefficients of the linear momentum and the air age. In the present simulations, it was considered $(\sigma_\tau = 1)$ [33].

Cooling efficiency of the ventilation system was examined using Cooling/Heating Efficiency Index Φ , a measure of the extent to which the cool supply air reaches the target point (e.g., occupied zone),

$$\Phi = \frac{T_p - T_{clo}}{T_s - T_{clo}} \quad (10)$$

III. Results and discussion

3.1. Verification and validation

A computational model was developed using the open-source CFD code (OpenFOAM). And a seated real shape manikin was used. In order to model the local airflow in the personal microenvironment of the human body, the configuration of the manikin was developed by [34, 35], and represented the real human used in the experiment.

A single cubicle case was created to represent the real cubicle. Hexahedral (hex-dominant) mesh was used in this study created using the utility (snappyHexMesh) provided with the software. SnappyHexMesh is a powerful meshing tool that can create a complex meshes with sophisticated, high controlled details in any location starting from basic hexahedral mesh and geometry surfaces.

To obtain valid simulation results, an appropriate mesh is necessary. Increasing the number of cells results in better accuracy as well as much more time for computing. Therefore an optimal mesh is necessary to balance time consumed and the accuracy of the calculation. Three meshes were created for the mesh independence study. A summary of the three grids is provided in Table 2. All the mesh cases consisted of hexahedral cells with quadratic surface elements, and prism layers attached on both manikin and walls boundaries (Fig. 9).

Table 2: Grid summary

	Coarse	Medium	Fine
Number of cells	2,123,867	2,400,945	3,370,392
Average y^+ on the manikin	1.92038	1.4366	1.3873
Average T at the outlet (T_R) [°C]	24.129	24.33	24.392
Average age of air at the outlet [sec]	155.94	152.1	151.7
Volume weighted mean PMV value [-]	0.39442	0.415841	0.415855

As shown in Table 2, the results of the medium and the fine mesh are very close. And knowing that the return air temperature in Kong's experiments was $T_R = 24.5$ °C [18], and after some compromising, the medium mesh can be considered as a valid mesh and its results will be used later.

3.2. Thermal comfort quantities

Since in the experiment, a real human was used instead of the manikin, a completely identical boundary condition could not be created in the CFD model. Instead, an approximation method was used to replace the thermal comfort boundary condition, a specified surfaces temperatures by body segment (based on [18]) with the same measured surface temperature of other objects was used (Table 3).

Table 3: Manikin and surfaces temperature

Part	Temperature °C	Part	Temperature °C
Face	30.0	Left upper thigh	32.0
Head	31.8	Right lower thigh	33.6
Shoulders	34.4	Left lower thigh	33.6
Right upper arm	31.4	Right leg	29.3
Left upper arm	31.4	Left leg	29.5
Right forearm	34.0	Right foot	29.2

Left forearm	33.7	Left foot	29.0
Right hand	32.5	Floor	22.6
Left hand	32.5	Celling	26.1
Chest	31.4	Monitor	25.7
Stomach	34.6	Computer case	25.9
Back	33.0	Walls	24.0
Right upper thigh	32.0	Supply air	18.4

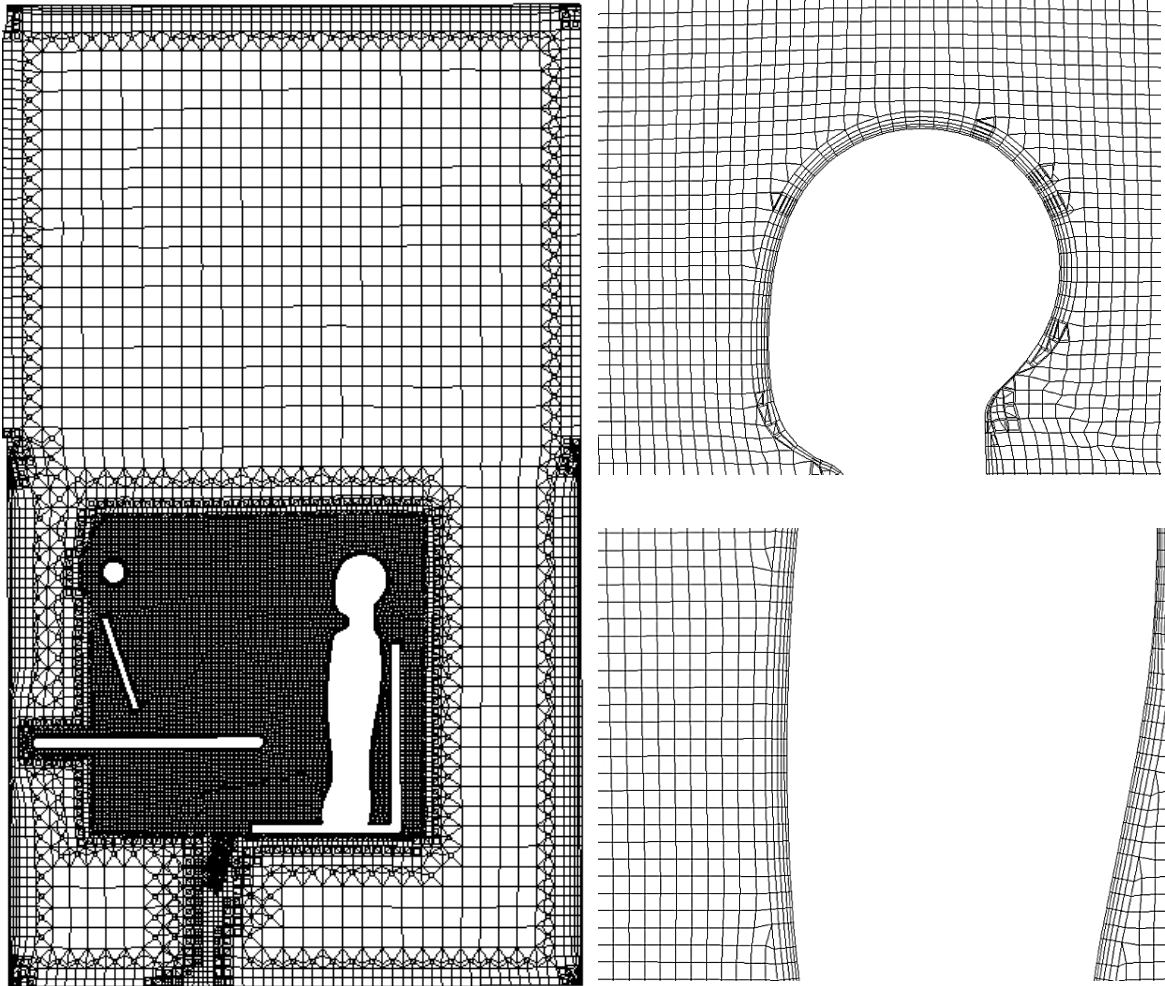


Fig.9: Mesh resolution

To evaluate the air quality, the concept age of air, AoA, was used, (Fig. 10) shows the iso-surface of the AoA of the value 5 sec colored by air temperature. The surface is covering the breathing zone, which means that the air within this surface is a new, fresh and contaminant free.

The cooling effect behaved similarly as the AoA. Cooler air was transported to the manikin's face directly with a little entrainment (to draw in and transport by the flow of a fluid), and part of the cooler air flowed around the head and then sank down to the floor level due to the heavier density caused by lower

temperature. Fig. 11 shows the cooling efficiency at the manikin symmetry plane with its good agreement compared to Kong's results [18].

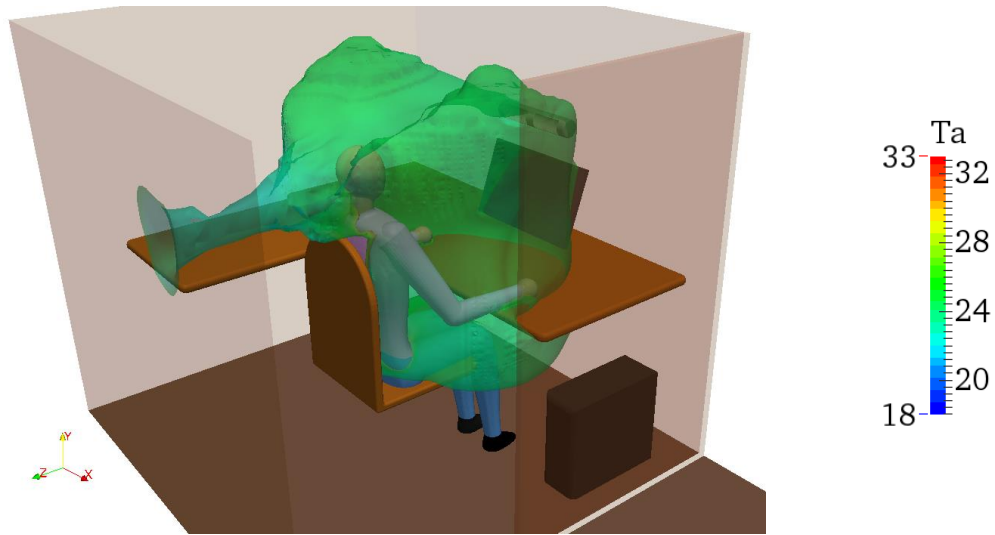


Fig.10: iso-surface AoA=5 sec (colored by air temperature)

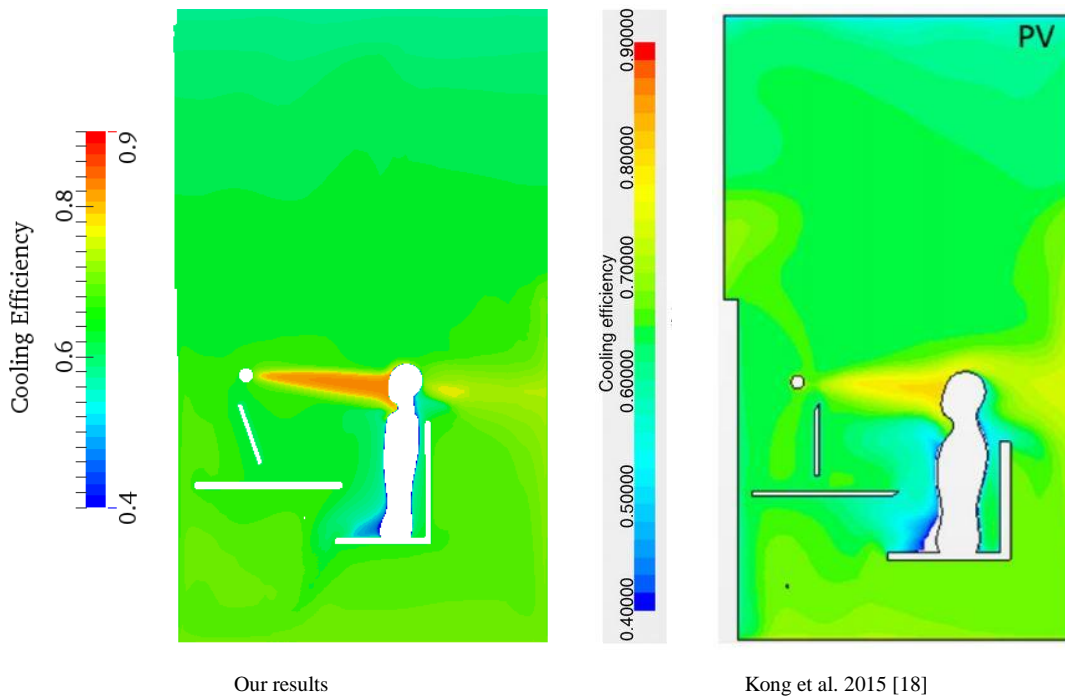


Fig.11: cooling efficiency at the manikin symmetry plane

The PMV was also calculated, and it is plotted on the manikin symmetry plane in (Fig. 12). A slightly cool region can be observed on the manikin face due to the concentration of the main air jet coming from the PV vent, and slightly warm regions located on the back, chest and stomach due to the lack of direct air flow. However, the volume weighted average of PMV was 0.415841, which is a comfortable thermal condition according to the standard ASHRAE 55-2010 [36].

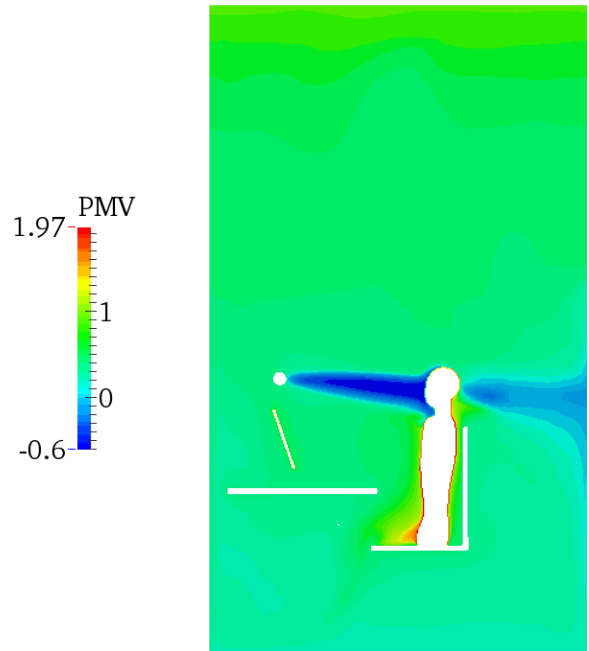


Fig.12: PMV at the manikin symmetry plane

3.3. Flow field quantities

The temperature and velocity fields also compared with Kong's results. (Fig. 13) shows the temperature distribution with respect to Kong's results, and (Fig. 14) shows the velocity distribution with respect to Kong's results, a good similarity between the results can be seen.

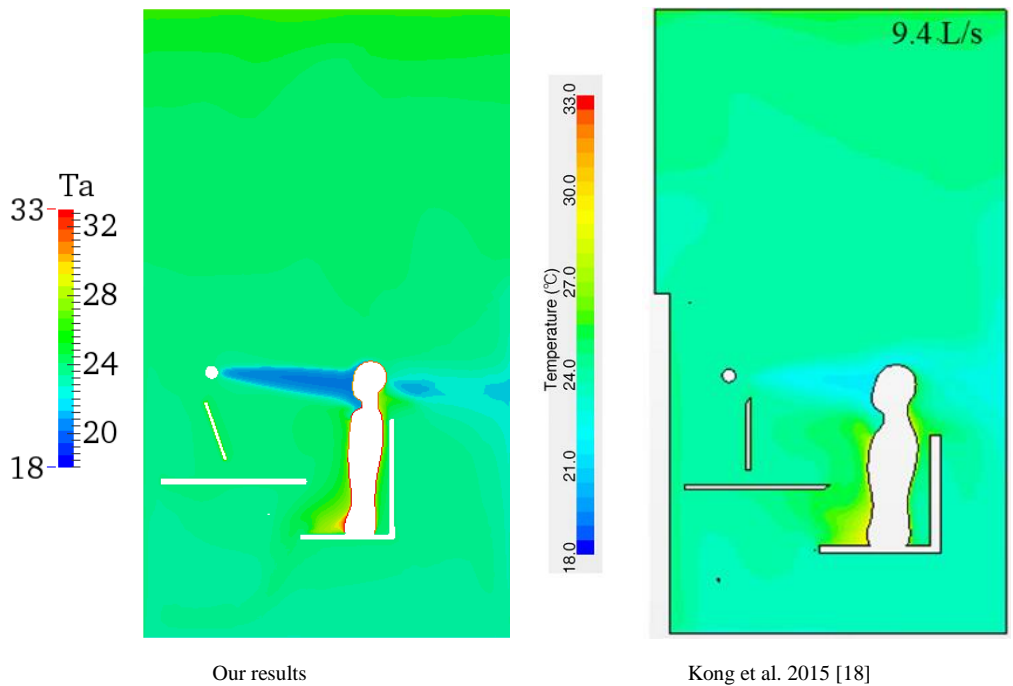


Fig.13: Temperature distribution at the manikin symmetry plane

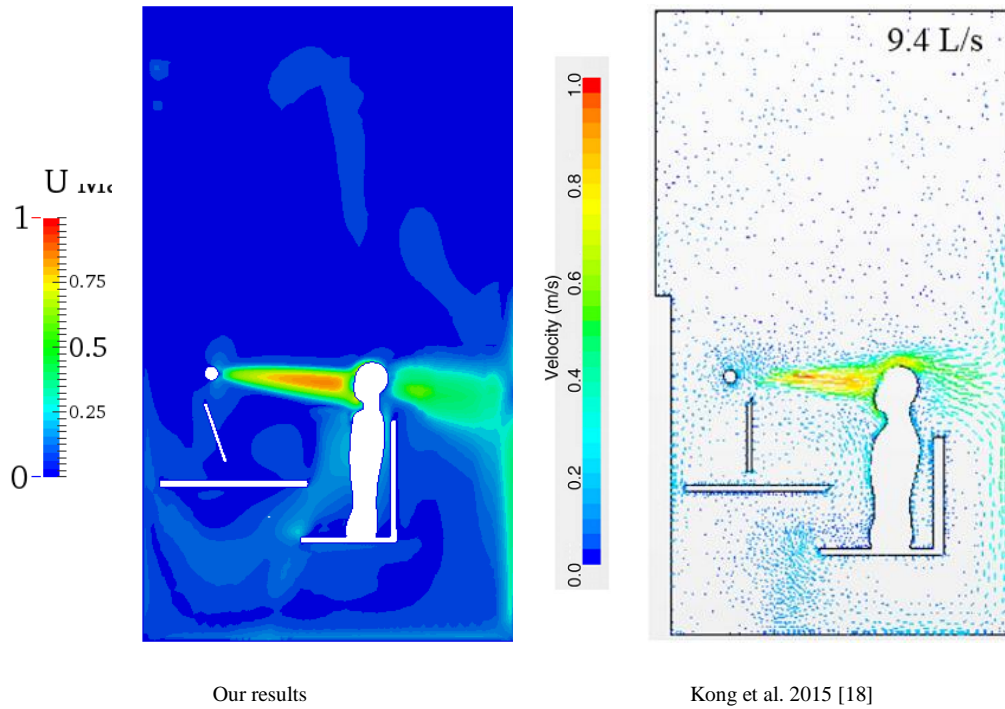


Fig.14: Velocity distribution at the manikin symmetry plane

Although Kong didn't specify the PV blades angles that describe the air direction, a similar flow field were established using our PV vent, also an experimental measurements couldn't be done. A numerical velocity profiles was plotted in the location FC and compared with Kong's results in (Fig. 15). The differences between numerical profiles can be related to the difference between the used PV vents.

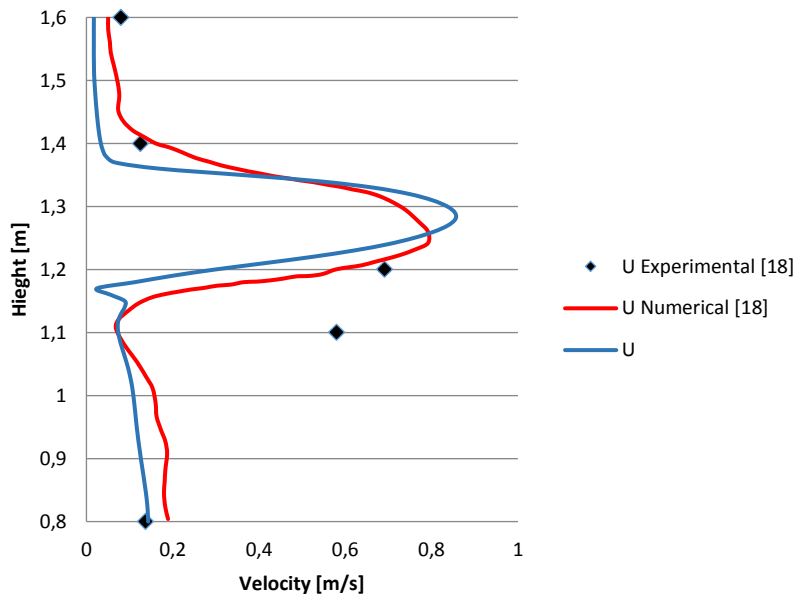


Fig.15: Velocity profiles in the location FC

As mentioned earlier, temperature was monitored in four location, however, temperature profile was only available in [18] at the location RF. (Fig. 16) shows the temperature profiles from the numerical results in the location RF and (Fig. 17) shows the experimental results.

The average relative error between the numerical temperature profiles was 0.56 %, and 1.01% in the experimental temperature profiles.

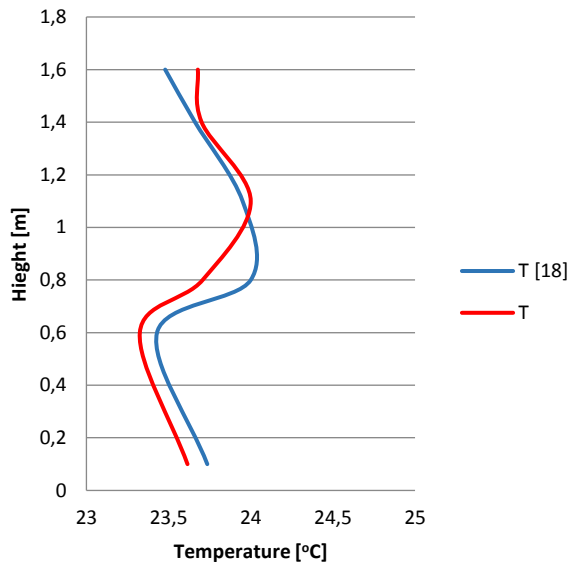


Fig.16: Temperature in location RF (numerical)

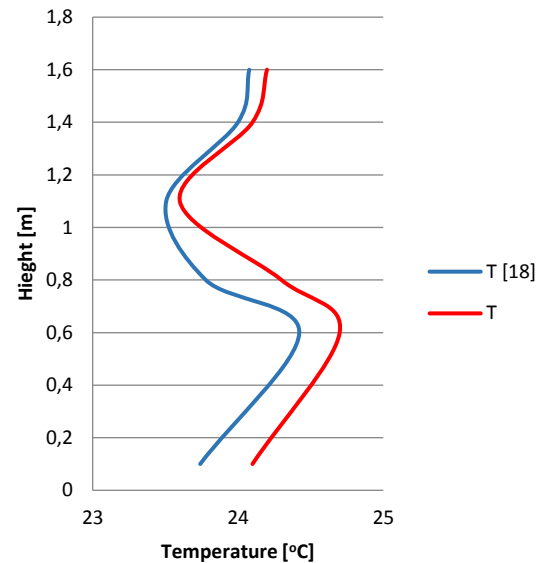


Fig.17: Temperature in location RF (experimental)

CONCLUSION

In this work, a numerical model was constructed. This model was able to predict the physical phenomena behind the flow in the cubicle and calculate the thermal comfort quantities correctly. The age of air, cooling efficiency and the predicted mean vote PMV were calculated using an additional library was added to the used software.

The numerical model was validated after performing a mesh independence study by comparing its basic flow parameters with the numerical results from Kong's research [18], the average relative error in the temperature profile was 0.56%.

An experimental model was also constructed and validated by comparing its results with Kong's experimental results, the average relative error in the temperature profile was 1.01%.

The main purpose of this work wasn't about comparing numerical and experimental results against each other, but to validate each one by its own. So, these models (numerical and experimental) can be used in further researches.

REFERENCES

- [1] Vander, A.J., J.H. Sherman, and D.S. Luciano, *Human physiology: the mechanisms of body function*. 1998: New York, US: McGraw-Hill, 1990.
- [2] Houdas, Y. and E. Ring, *Human body temperature-Its measurement and regulation*. 1982.
- [3] Dygert, R.K., et al., *Modeling of the Human Body to Study the Personal Micro Environment*. 2009. **115**(2).
- [4] Melikov, A.K., et al., *Personalized ventilation: evaluation of different air terminal devices*. 2002. **34**(8): p. 829-836.

- [5] Kaczmarczyk, J., A. Melikov, and P.O.J.I.A. Fanger, *Human response to personalized ventilation and mixing ventilation*. 2004. **14**: p. 17-29.
- [6] Gao, N., J.J.H. Niu, and R. Research, *Modeling the performance of personalized ventilation under different conditions of room air and personalized air*. 2005. **11**(4): p. 587-602.
- [7] Cermak, R., et al., *Performance of personalized ventilation in conjunction with mixing and displacement ventilation*. 2006. **12**(2): p. 295-311.
- [8] Chludzinska, M. and A.J.C. Bogdan, Ogrzewnictwo, Wentylacja, *Individual ventilation—Users' whim or economically justified energy saving*. 2008. **2**: p. 32-34.
- [9] Melikov, A.K. *Improving comfort and health with personalized ventilation*. in *9th International Conference on Air Distribution in Rooms*. 2004. University of Coimbra.
- [10] Melikov, A.K., V.J.H. Dzhartov, and R. Research, *Advanced air distribution for minimizing airborne cross-infection in aircraft cabins*. 2013. **19**(8): p. 926-933.
- [11] Dygert, R.K., T.Q.J.B. Dang, and Environment, *Experimental validation of local exhaust strategies for improved IAQ in aircraft cabins*. 2012. **47**: p. 76-88.
- [12] Nielsen, P.V., et al., *The influence of draught on a seat with integrated personalized ventilation*. 2008: p. 17-22.
- [13] Nielsen, P.V., et al. *Chair with Integrated Personalized Ventilation for Minimizing Cross Infection*. in *The International Conference on Air Distribution in Rooms, Roomvent*. 2007. FINVAC ry.
- [14] Nielsen, P.V., et al. *Test of different air distribution concepts for a single-aisle aircraft cabin*. in *CLIMA 2013REHVA World Congress*. 2013. Society of Environmental Engineering (STP).
- [15] Nielsen, P.V., et al., *Personal exposure between people in a room ventilated by textile terminals—with and without personalized ventilation*. 2007. **13**(4): p. 635-643.
- [16] Nielsen, P.V., H. Jiang, and M. Polak. *Bed with Integrated Personalized Ventilation for Minimizing Cross Infection*. in *The International Conference on Air Distribution in Rooms, Roomvent*. 2007. FINVAC ry.
- [17] Zhuang, R., X. Li, and J. Tu. *CFD study of the effects of furniture layout on indoor air quality under typical office ventilation schemes*. in *Building Simulation*. 2014. Springer.
- [18] Kong, M., J. Zhang, and J. Wang. *Air and air contaminant flows in office cubicles with and without personal ventilation: A CFD modeling and simulation study*. in *Building Simulation*. 2015. Springer.
- [19] Russo, J., *A detailed and systematic investigation of personal ventilation systems*. 2011.
- [20] Chen, Q., W.J.E. Xu, and buildings, *A zero-equation turbulence model for indoor airflow simulation*. 1998. **28**(2): p. 137-144.
- [21] Gao, N., J.J.B. Niu, and Environment, *CFD study on micro-environment around human body and personalized ventilation*. 2004. **39**(7): p. 795-805.
- [22] Hayashi, T., et al., *CFD analysis on characteristics of contaminated indoor air ventilation and its application in the evaluation of the effects of contaminant inhalation by a human occupant*. 2002. **37**(3): p. 219-230.
- [23] Gao, N., J.J.B. Niu, and Environment, *Transient CFD simulation of the respiration process and inter-person exposure assessment*. 2006. **41**(9): p. 1214-1222.
- [24] Khalifa, H.E., et al. *Computation of occupant exposure in an office cubicle*. in *Proceedings of AWMA/EPA Conference: Indoor Air Quality—Problems, Research and Solutions, Durham, USA*. 2006.
- [25] Dang, T.J.U.P.P., *Personalized ventilation system using combined jet nozzle and flow suction*. 2008(61/022956).
- [26] Russo, J.S., et al., *Computational analysis of reduced-mixing personal ventilation jets*. 2009. **44**(8): p. 1559-1567.
- [27] Deevy, M., et al., *Modelling the effect of an occupant on displacement ventilation with computational fluid dynamics*. 2008. **40**(3): p. 255-264.
- [28] Xu, W., Q.J.E. Chen, and Buildings, *A two-layer turbulence model for simulating indoor airflow: Part II. Applications*. 2001. **33**(6): p. 627-639.
- [29] Xu, W. and Q.J.I.a. Chen, *Simulation of mixed convection flow in a room with a two-layer turbulence model*. 2000. **10**(4): p. 306-314.
- [30] Open, C., OpenFOAM Foundation, *OpenFOAM user guide*. 2011. **2**(1).
- [31] Iso, E.J.E.o.t.t.e.-A.d., et al., *7730: 2005*. 2005.
- [32] Fanger, P.O.J.T.c.A. and a.i.e. engineering., *Thermal comfort. Analysis and applications in environmental engineering*. 1970.
- [33] Li, X., et al., *Total air age: an extension of the air age concept*. 2003. **38**(11): p. 1263-1269.
- [34] Khalifa, H.E., et al., *Experimental investigation of reduced-mixing personal ventilation jets*. 2009. **44**(8): p. 1551-1558.
- [35] Villi, G. and M. De Carli. *Detailing the effects of geometry approximation and grid simplification on the capability of a CFD model to address the benchmark test case for flow around a computer simulated person*. in *Building Simulation*. 2014. Springer.
- [36] American Society of Heating, R. and A.-C. Engineers, *Thermal Environmental Conditions for Human Occupancy: ANSI/ASHRAE Standard 55-2013 (supersedes ANSI/ASHRAE Standard 55-2010)*. 2010: American Society of Heating, Refrigerating, and Air-Conditioning Engineers.